Control of K+ channel gating by protein phosphorylation: structural switches of the inactivation gate

Christoph Antz[1], Tanja Bauer[2], Hubert Kalbacher[2], Rainer Frank[3], Manuel Covarrubias[4], Hans Robert Kalbitzer[5], Johann Peter Ruppersberg[1], Thomas Baukrowitz[1] and Bernd Fakler[1]

[1]Department of Physiology II, University of Tübingen, Ob dem Himmelreich 7, 72074 Tübingen, Germany. [2]Institute of Physiological Chemistry, University of Tübingen, Ob dem Himmelreich 7, 72074 Tübingen, Germany. [3]Zentrum für Molekulare Biologie, Im Neuenheimer Feld, 69120 Heidelberg, Germany. [4]Department of Pathology, Anatomy and Cell Biology, Jefferson Medical College, 1020 Locust St JAH 245, Philadelphia, Pennsylvania 19107, USA. [5]Department of Biophysics and Physical Biochemistry, University of Regensburg, Universitätsstr. 31, 93053 Regensburg, Germany.

Fast N-type inactivation of voltage-dependent potassium (K_v) channels controls membrane excitability and signal propagation in central neurons and occurs by a 'ball-and-chain'-type mechanism. In this mechanism an N-terminal protein domain (inactivation gate) occludes the pore from the cytoplasmic side. In K_v3.4 channels, inactivation is not fixed but is dynamically regulated by protein phosphorylation. Phosphorylation of several identified serine residues on the inactivation gate leads to reduction or removal of fast inactivation. Here, we investigate the structure-function basis of this phospho-regulation with nuclear magnetic resonance (NMR) spectroscopy and patch-clamp recordings using synthetic inactivation domains (ID). The dephosphorylated ID exhibited compact structure and displayed high-affinity binding to its receptor. Phosphorylation of serine residues in the N- or C-terminal half of the ID resulted in a loss of overall structural stability. However, depending on the residue(s) phosphorylated, distinct structural elements remained stable. These structural changes correlate with the distinct changes in binding and unbinding kinetics underlying the reduced inactivation potency of phosphorylated IDs.

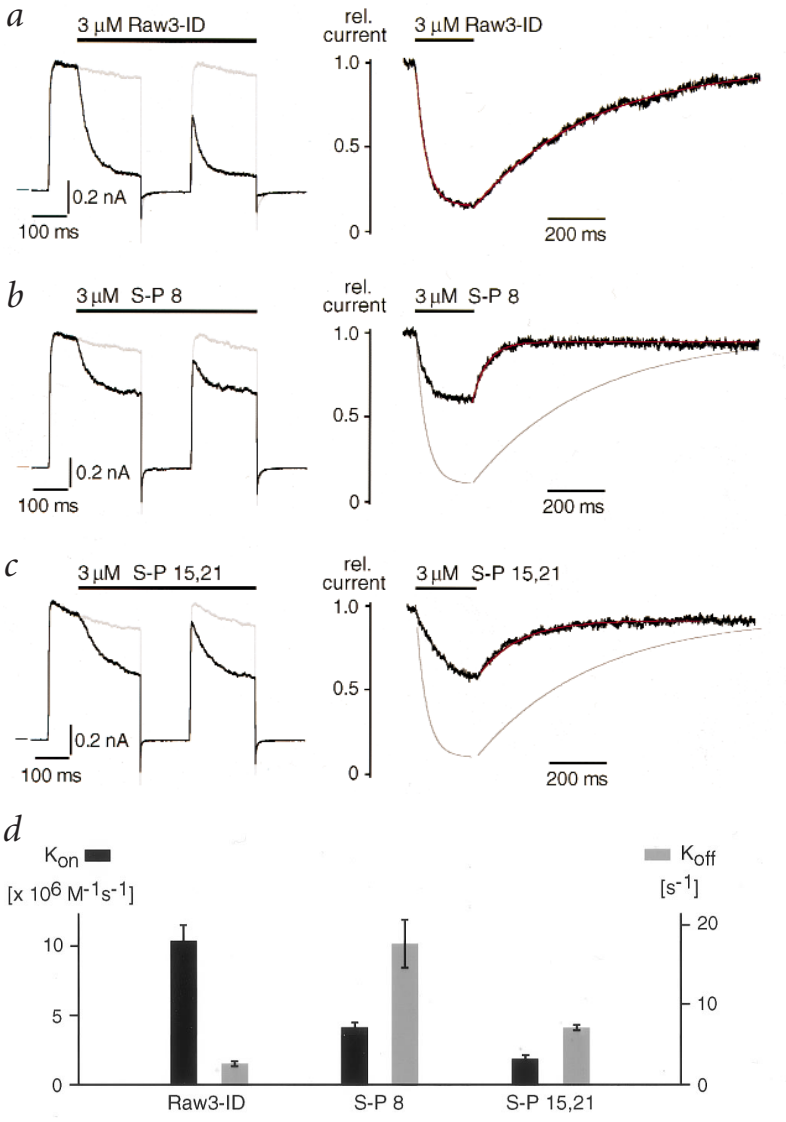

Fig. 1 Effect of phosphorylation on inactivation kinetics is site specific. ***a*** (left panel), Inactivation of non-inactivating K_v1.1 channels mediated by 3 µM dephospho Raw3-ID applied to the cytoplasmic side of a giant inside-out patch. Current trace, recorded with the peptide applied (application as indicated by the horizontal bar), is in black; control trace is in gray. The first part of the recording is inactivation by rapid application of the peptide (see Methods, solution exchange <2 ms), the second part is inactivation in the continuous presence of Raw3-ID. Outward currents were elicited by voltage steps from -120 mV to 0 mV; [K^+] was 120 mM on the cytoplasmic side and 5 mM on the extracellular side. Scale bars are as indicated. (right panel), Application and wash-off of 3 µM Raw3-ID. Current was normalized to the control trace and a monoexponential (line) fitted to the wash-in and wash-off, respectively. Time constants obtained from the fits were 34.5 ms for wash-in and 406 ms for wash-off. ***b***,***c***, Inactivation induced by S-P 8 and S-P 15,21. Experimental conditions as in (*a*). In the right panel, fit lines from (*a*) were added for better comparison. Time constants obtained from fits to the wash-off (line) were 50.7 ms and 141.3 ms for S-P 8 and S-P 15,21, respectively. ***d***, Rates of the inactivation process mediated by Raw 3-ID and the two phospho IDs. Values are mean ± s.d from five to seven experiments. Note the differential effect of the two phosphorylations on k_{on} and k_{off}, respectively. Binding affinity for the various IDs was 0.26 ± 0.04 µM for Raw3-ID, 4.34 ± 0.96 µM for S-P 8 and 4.11 ± 0.79 µM for S-P 15,21.

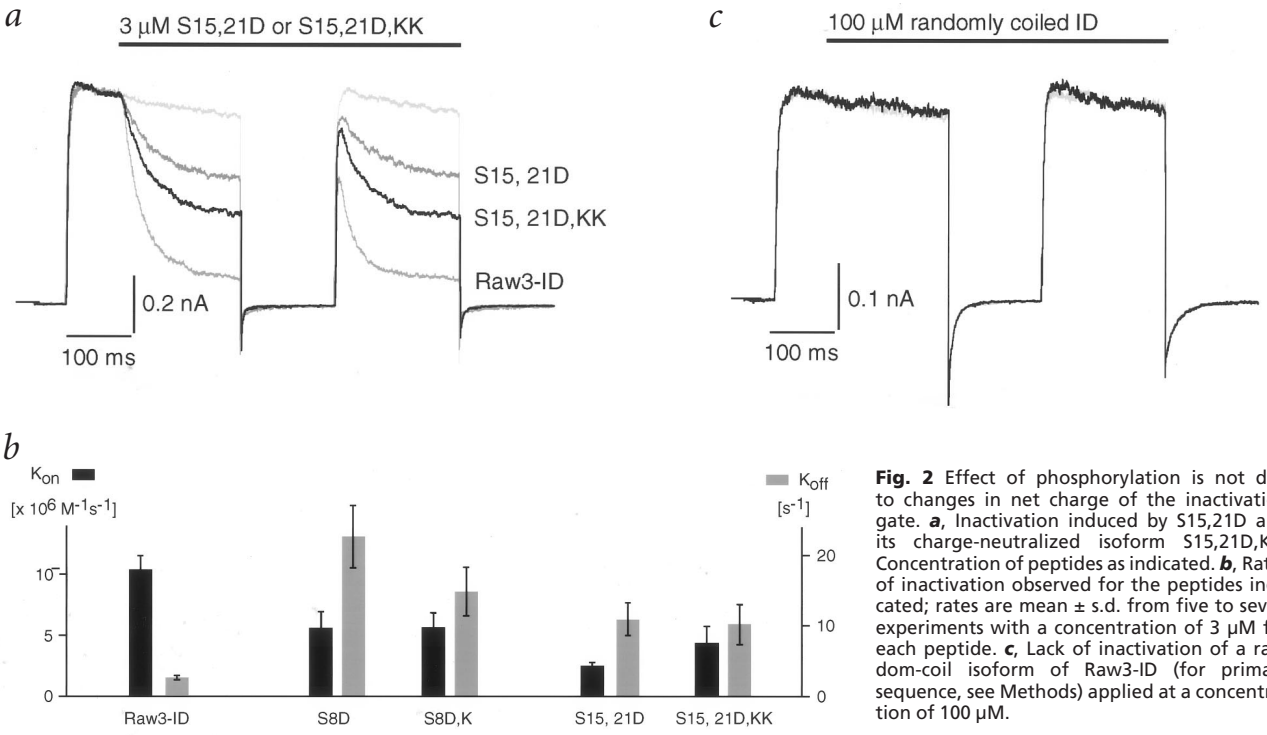

Fig. 2 Effect of phosphorylation is not due to changes in net charge of the inactivation gate. ***a***, Inactivation induced by S15,21D and its charge-neutralized isoform S15,21D,KK. Concentration of peptides as indicated. ***b***, Rates of inactivation observed for the peptides indicated; rates are mean ± s.d. from five to seven experiments with a concentration of 3 μM for each peptide. ***c***, Lack of inactivation of a random-coil isoform of Raw3-ID (for primary sequence, see Methods) applied at a concentration of 100 μM.

Protein phosphorylation is a prevalent cellular mechanism for modulating the gating properties of ion channels[1–4], but only little is known about the structure-function basis of these phospho-regulations. In K_v3.4 (Raw3) channels, phosphorylation by protein kinase C (PKC) controls N-type inactivation[5,6], which represents the best-understood gating transition in ion channels[7–10]. In this gating process a cytoplasmic ID (amino acids 1–30 in K_v3.4)[11] binds to a receptor site that is located in the inner vestibule of the channel and is accessible only when the pore is open[12]. The ID of K_v3.4 (Raw3-ID) has been structurally characterized to a resolution of 1.3 Å and found to exhibit compact folding in aqueous solution[13]. As for all known IDs, Raw3-ID is able to induce inactivation in non-inactivating K_v channels even when applied as a synthetic peptide[10,14,15].

Application of synthetic IDs to non-inactivating K_v1.1 channels in inside-out patches from *Xenopus* oocytes was used to analyze the functional properties of phospho and dephospho IDs (Fig. 1). Application and wash-off of the peptides was accomplished by a piezo-controlled 'fast-application system' (see Methods), which allowed solution exchange at giant inside-out patches in <2 ms[16]. Rapid application and wash-off (Fig. 1*a*, right panel) of 3 μM dephospho Raw3-ID was achieved. Inactivation occurred with a time constant of ~30 ms and was the same whether determined by fast application (Fig. 1*a*, left panel, first activation) or in the continuous presence of the peptide (Fig. 1*a*, left panel, second activation). In contrast to inactivation, wash-off of Raw3-ID, which should reflect unbinding of the peptide from the receptor, was slow and could be well fit with a monoexponential (Fig. 1*a*, right panel). This indicates that the ID–receptor interaction is indeed a first-order reaction[10], with on and off rates (k_{on}, k_{off}) calculated as 10.2×10^6 M^{-1} s^{-1} and 2.6 s^{-1} for the dephospho Raw3-ID (Fig. 1*d*).

Based on these results, we analyzed the effect of phosphorylation on inactivation kinetics. Two different phosphopeptides were examined: one phosphorylated at Ser 8 located in the N-terminal half of Raw3-ID (S-P 8), and one phosphorylated at residues Ser 15 and Ser 21 located in the C-terminal half of the molecule (S-P 15,21). Steady-state inactivation was largely reduced by phosphorylation in either half of the ID (40 ± 3% for S-P 8 and 43 ± 3 % for S-P 15,21; Fig. 1*b,c*). The on-off kinetics, however, differed significantly between S-P 8 and S-P 15,21 (Fig.1*b,c*). While phosphorylation at Ser 8 predominantly increased k_{off} (6.7-fold compared to Raw3-ID), addition of phosphate groups to residues Ser 15 and Ser 21 mainly decreased k_{on} (5.7-fold; Fig. 1*d*). Thus, phosphorylation at distinct residues resulted in distinct changes of the inactivation kinetics.

Since phosphoserine(s) introduces negative charges (usually one to two per phosphoamino acid[17]) into the ID and are known to promote structural responses[17], we investigated whether the observed kinetic effects are based on changes in net charge or changes in structure of the ID. Possible charge effects were tested by comparing IDs with serine to aspartate mutations (S8D, S15,21D), which mimic phosphorylation when made in the inactivation domain of K_v3.4 channels[5,6], to peptides with the S–D mutation(s) and lysine residues added at their C-termini for net charge neutralization (S8D,K and S15,21D,KK). As seen on recordings obtained with 3 μM S15,21D and S15,21D,KK, net charge neutralization failed to compensate for the effect of the S–D exchange, although it led to an increase in steady-state inactivation (Fig. 2*a*, 52 ± 3%). Kinetic analysis showed that both peptides S8D and S15,21D closely resembled the respective

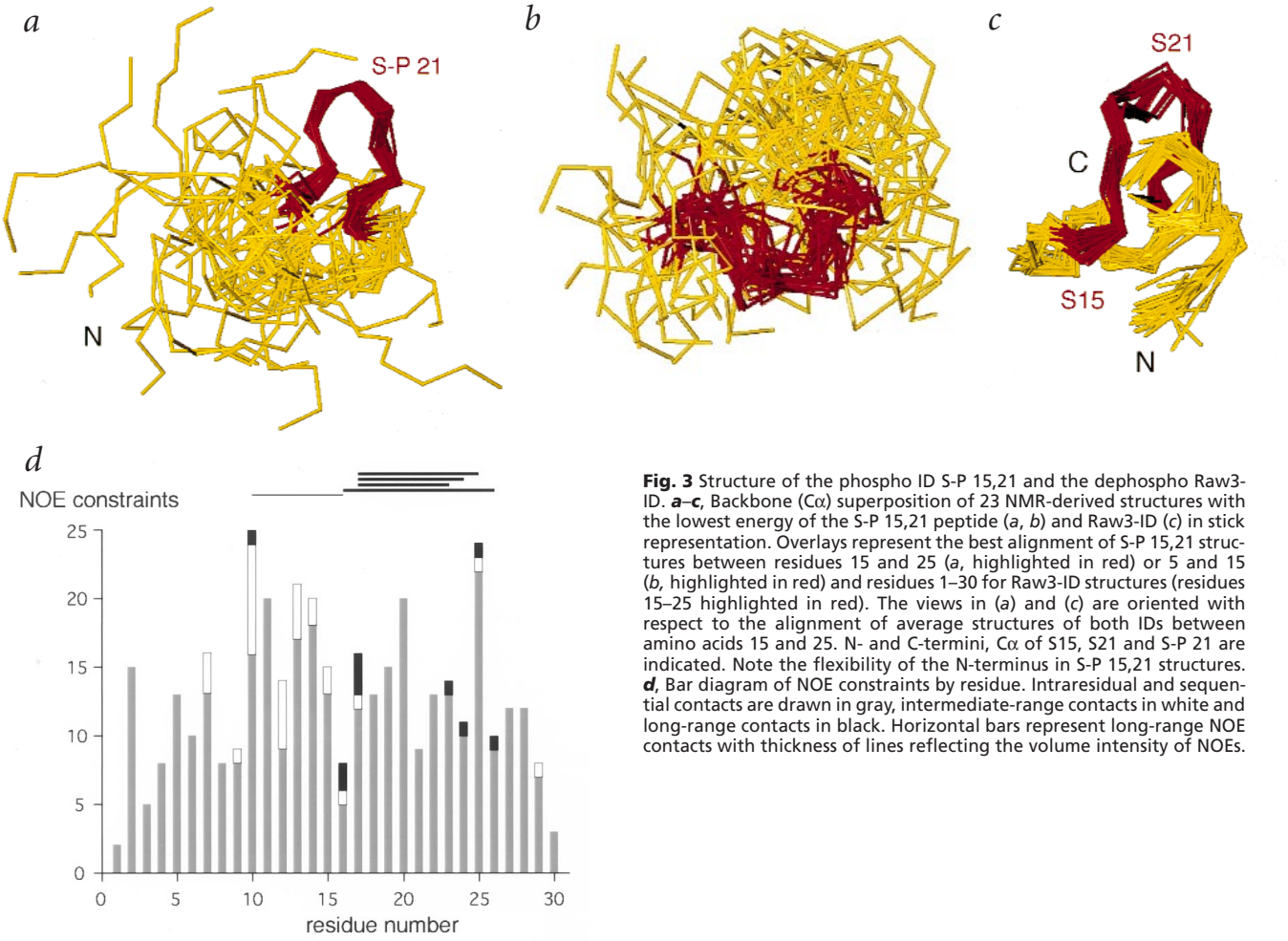

Fig. 3 Structure of the phospho ID S-P 15,21 and the dephospho Raw3-ID. ***a–c***, Backbone (Cα) superposition of 23 NMR-derived structures with the lowest energy of the S-P 15,21 peptide (*a*, *b*) and Raw3-ID (*c*) in stick representation. Overlays represent the best alignment of S-P 15,21 structures between residues 15 and 25 (*a*, highlighted in red) or 5 and 15 (*b*, highlighted in red) and residues 1–30 for Raw3-ID structures (residues 15–25 highlighted in red). The views in (*a*) and (*c*) are oriented with respect to the alignment of average structures of both IDs between amino acids 15 and 25. N- and C-termini, Cα of S15, S21 and S-P 21 are indicated. Note the flexibility of the N-terminus in S-P 15,21 structures. ***d***, Bar diagram of NOE constraints by residue. Intraresidual and sequential contacts are drawn in gray, intermediate-range contacts in white and long-range contacts in black. Horizontal bars represent long-range NOE contacts with thickness of lines reflecting the volume intensity of NOEs.

phospho IDs and that charge neutralization could not reverse the effect of S–D mutations on k_{on} and k_{off} (Fig. 2*b*).

These results indicate that changes in net charge alone cannot account for the phosphorylation effects and suggest a structural basis for the effects. This is supported by a peptide composed of the same amino acids as Raw3-ID but with changed primary sequence (see Methods). This peptide exhibited random-coil structure as determined in NMR experiments (data not shown) and failed to induce any inactivation even when applied at 100 μM (Fig. 2*c*).

Since a change in structure rather than in net charge gave rise to changes in function, we analyzed the phospho IDs S-P 8 and S-P 15,21 in aqueous solution (at two pHs and ionic strengths; see Methods) with NMR spectroscopy (Figs 3 and 4, Table 1). Addition of phosphate groups at S15 and S21 (Fig. 3*a,b*) largely destabilized the overall compact folding exhibited by the dephospho ID (Fig. 3*c*). The structure of the S-P 15,21 peptide consisted of two parts, a highly ordered loop structure formed by amino acids 15–25 (highlighted in red in Fig. 3*a*) and a less ordered and flexible N-terminus, comprising amino acids 1–14 (highlighted in red in Fig. 3*b*). These structurally different domains are reflected by the observed NOE patterns, showing long-range connectivities between residues 16 and 17 and amino acids 23–26 (Fig. 3*d*). Moreover, the disordered (mobile) part of the structure is characterized by missing of NOEs defining a unique fold and by chemical shift values typical for random-coil peptides[18]. The loop structure, which was well defined with values for the r.m.s. deviation to the mean structure of 0.67 Å for backbone atoms and 1.60 Å for all atoms, is very similar to that formed by the same amino acids in the dephospho ID (Fig. 3*c*). Interestingly, structural conservation occurred close to the phosphorylated serine residues, while disturbance in backbone conformation was seen in more distant parts. The driving force underlying the structural rearrangements in the S-P 15,21 peptide, as compared to the dephospho ID, may be steric interactions between the phosphate groups and spatially close residues or electrostatic interactions between the phosphate groups and residues Glu 27, Glu 28, which are spatially close in the dephospho structure[13]. Similarly to phosphorylation of the C-terminal residues, introduction of a phosphoserine at position 8 resulted in an overall destabilization of the ID structure (Fig. 4). In contrast to S-P 15,21, however, the C-terminus between amino acids 15 and 30 was found to be disordered and flexible (Fig. 4*a,b*, Table 1); the long-range NOE contacts observed in S-P 15,21 were absent (Fig. 4*d*). In addition, the chemical shifts suggest an unfolded structure. The N-terminus of the S-P 8 peptide was composed of a flexible region at its very end (amino acids 1–5) and an ordered region between amino acids 5 and 15 (highlighted in red and cyan in Fig. 4*a*). The backbone conformation of the latter was well defined in the NMR structure (r.m.s.deviation values of 1.09 Å for backbone atoms and 2.16

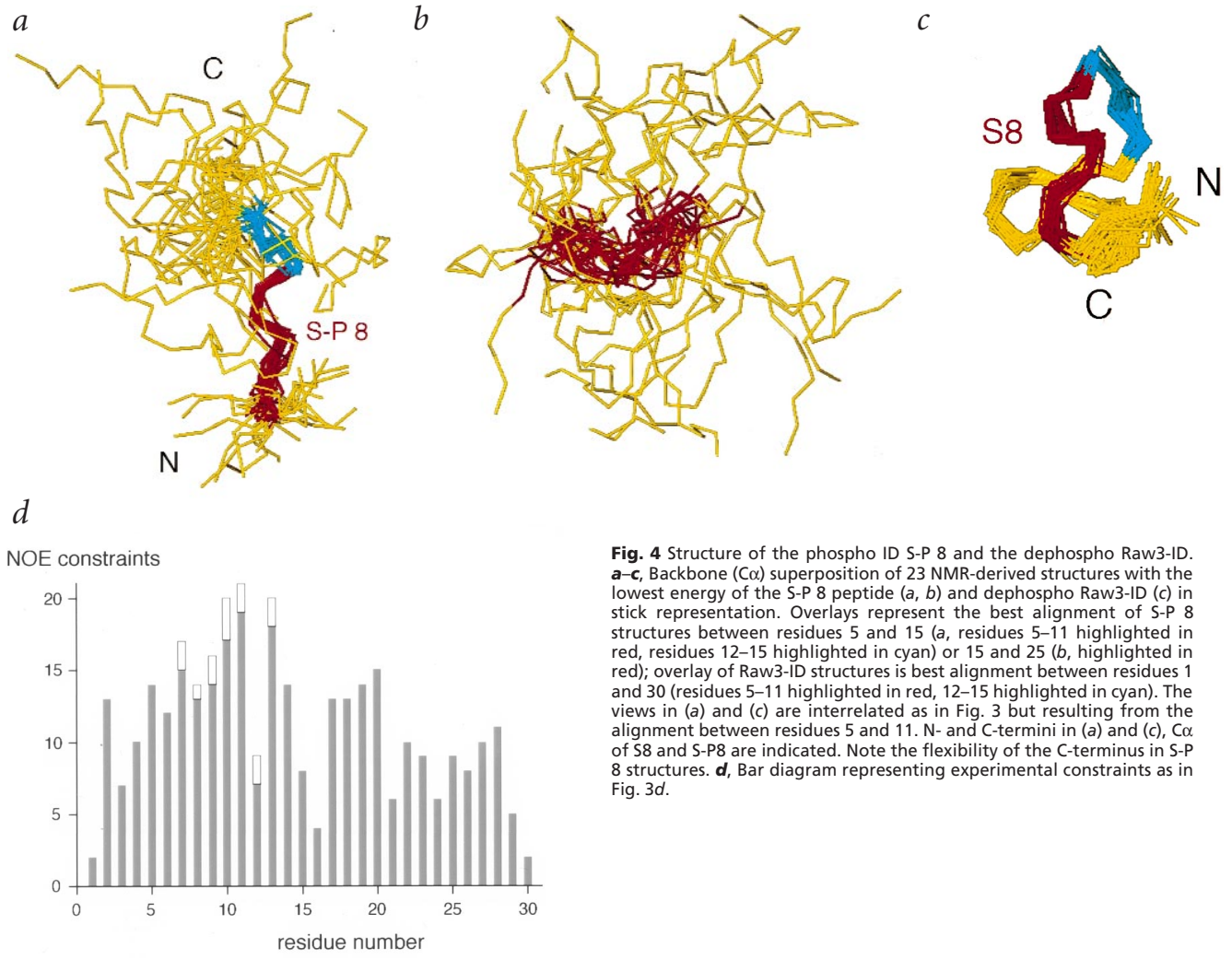

Fig. 4 Structure of the phospho ID S-P 8 and the dephospho Raw3-ID. ***a*–*c***, Backbone (Cα) superposition of 23 NMR-derived structures with the lowest energy of the S-P 8 peptide (*a*, *b*) and dephospho Raw3-ID (*c*) in stick representation. Overlays represent the best alignment of S-P 8 structures between residues 5 and 15 (*a*, residues 5–11 highlighted in red, residues 12–15 highlighted in cyan) or 15 and 25 (*b*, highlighted in red); overlay of Raw3-ID structures is best alignment between residues 1 and 30 (residues 5–11 highlighted in red, 12–15 highlighted in cyan). The views in (*a*) and (*c*) are interrelated as in Fig. 3 but resulting from the alignment between residues 5 and 11. N- and C-termini in (*a*) and (*c*), Cα of S8 and S-P8 are indicated. Note the flexibility of the C-terminus in S-P 8 structures. ***d***, Bar diagram representing experimental constraints as in Fig. 3*d*.

Å for all atoms) and showed some similarity to the corresponding region in the dephospho ID (Fig. 4*a*,*c*).

Thus, introduction of phosphate groups resulted in structural rearrangements in both phospho IDs: similar observations have recently been reported for other proteins[19,20]. These rearrangements were different in S-P 15,21 and S-P 8, as were the inactivation kinetics observed between the two phosphopeptides and between phospho and dephospho IDs (Figs 1, 2). The correlation of structural and functional data suggests that the gate–receptor interaction in the ID-bound state is mainly mediated by the C-terminal hemisphere of Raw3-ID. This is reflected by unfolding of this region in the S-P 8 peptide, which resulted in a large increase of k_{off} and by its partial disturbance in S-P 15,21, accompanied by only a moderate increase in k_{off}. The N-terminal hemisphere seems to determine k_{on}, as is reflected by its gradual disturbance in the phospho IDs and the concomitant reduction in k_{on} of inactivation.

In conclusion, we find that the mechanism underlying phospho-regulation of fast inactivation in $K_v3.4$ channels is a structural rearrangement of the inactivation gate that distinctly alters inactivation kinetics depending on the residue phosphorylated. Physiologically, these distinct alterations should have direct implication for the electrical activity in central neurons[21]. Thus, an increase in k_{off}, as results from phosphorylation of Ser 8, will lead to a faster recovery from N-type inactivation, which in turn will more rapidly terminate a train of action potentials (spike interval)[22,23]. A decreased k_{on} of N-type inactivation as observed for phosphorylation at residues Ser 15 and Ser 21 will hinder propagation of action potentials and result in an elongated interspike interval[22,23].

Methods

Electrophysiology. $K_v1.1$ channels were heterologously expressed in *Xenopus* oocytes as described[24]. Giant-patch recordings were made at room temperature (~23 °C) three to seven days after injection of $K_v1.1$-specific cRNA. Pipettes used were made from thick-walled borosilicate glass, had resistances of 0.3–0.6 MΩ (tip diameter of ~20 µm) and were filled with 5 mM KCl, 115 mM NaCl, 10 mM HEPES and 1.8 mM $CaCl_2$, pH 7.2. Currents were sampled at 10 kHz and corrected for capacitive transients with an EPC9 amplifier (HEKA Electronics), with analog filter set to 3 kHz (-3 dB). The fast-application system consists of a double-barrel pipette (tip opening of ~60 µm) mounted on a piezo, which could be moved by voltage steps in <80 µs. With giant inside-out patches placed directly in front of the application pipette, this device allowed for a complete solution exchange in <2 ms, as tested by the exchange (wash-in and wash-off) of K^+ versus Na^+ ions in activated $K_v1.1$ channels. Peptides were dissolved in K_{int} solution and applied through one

barrel of the application system; K_{int} consisted of the following: 120 mM KCl, 10 mM HEPES, 10 mM EGTA, 0.1 mM dithiothreitol, pH 7.2. Rates of inactivation were calculated from the results of monoexponential fits to the measured time courses of wash-in and wash-off of the peptides. K_{off} was determined from the time constant of the wash-off (τ_{off}) as $k_{off} = 1 / \tau_{off}$. According to a pseudo-first-order reaction, k_{on} was then calculated as $k_{on} = (1 / \tau_{on} - k_{off}) / [peptide]$, with τ_{on} the time constant for wash-in[16]. Affinity for peptide–receptor interaction was calculated as k_{off} / k_{on}. All values are given as mean ± s.d. of five to seven experiments.

Peptide synthesis. Peptides were made by conventional solid-phase synthesis and purified by HPLC[25]. For the synthesis of S-P 8 and S-P 15,21, serine residues were substituted by phosphoserines. Dephospho and phospho IDs had the following primary sequence: MISSVCV**SS**YRGRK**S**GNKPP**S**KTCLKEEMA (serine residues targeted by phosphorylation are in bold). The 'random-coil' isoform of Raw3-ID (Fig. 2*c*) had the following sequence: RMISRSVCEVSSKYGSKGNPKPSTKCLMEA.

Table 1 Structural statistics of S-P 8 and S-P 15,21

	S-P 8	S-P 15,21
Total number of distance constraints	247	274
Intraresidual	162	173
Sequential	78	84
Intermediate (|i - j| ≤ 4)	7	13
Long range (|i - j| > 4)	0	4
Dihedral angle constraints	27	25
Distance constraint violations >0.5 Å (per conformer)	0	0
Dihedral angle constraint violations >5 (per conformer)	0	0
Average total X-PLOR energy (kJ mol^{-1})	-21.4	-33.8
Average pairwise r.m.s. deviation from distance constraints	0.29 Å	0.25 Å
Average pairwise r.m.s. deviation from dihedral constraints	0.32	0.05
Average pairwise r.m.s. deviation from covalent bonds	0.004 Å	0.004 Å
Average pairwise r.m.s. deviation from covalent angles	0.63	0.67

R.m.s. deviation values from the mean structure

	S-P 8		S-P 15,21	
Residue number	Backbone atoms	All atoms	Backbone atoms	All atoms
1–30	5.80 Å	6.66 Å	4.50 Å	5.46 Å
5–15	1.09 Å	2.16 Å	2.13 Å	3.39 Å
15–25	2.78 Å	4.06 Å	0.67 Å	1.60 Å

Sample preparation for NMR. All peptides were dissolved in 0.5 ml 99.9% D_2O and in a mixture of 90% H_2O/10% D_2O (v/v), respectively; final concentrations were 2.0 mM at pH 3.5 for S-P 8, 2.0 mM at pH 3.4 for S-P 15,21 and 2.0 mM at pH 3.3 for the random-coil isoform of Raw3-ID. For verification of structural stability under physiological conditions, all peptides were also dissolved at pH 6.8 in a buffer solution suited for NMR spectroscopy with physiological ionic strength and ion composition[26].

NMR spectroscopy. NMR spectra were recorded at 283 K with a Bruker AMX-500 spectrometer. ^{1}H chemical shifts were referred to 2,2-dimethyl-2-silapentane-5-sulfonate (DSS). Spin system identification and sequential assignments were achieved by two-dimensional homonuclear NOESY[27], DQF-COSY[28] and TOCSY[29] experiments. TOCSY experiments were recorded with a mixing time of 60 ms. To identify spin diffusion effects, NOESY spectra with mixing times between 50 and 250 ms were recorded. $^3J_H{}^N{}_H{}^\alpha$ coupling constants were measured in high-resolution DQF-COSY experiments with a digital resolution of 0.66 Hz/pt.^{31}P 1D spectra were recorded for verification of the peptide synthesis in S-P 8 and S-P 15,21. Comparison of NOESY and TOCSY spectra recorded from S-P 8 and S-P 15,21 at pH 6.8 and acidic pH values showed no significant changes in resonance shifts for aliphatic groups (except for titratable residues) and NOE distributions.

Structure calculations. Structures were calculated with the program X-PLOR 3.851[30]. For both phospho IDs, 500 starting structures were generated from a random field of atomic coordinates with a subsequent regularization and minimization. The target function that was minimized during simulated annealing[31] and restrained molecular dynamic simulations comprises quadratic harmonic potential terms for the covalent geometry, angles, torsions, and improper terms and a 6-12 Lennard-Jones or soft quartic potential with a cut-off at 8 Å for the van der Waals repulsion term. An additional conventional coulomb potential with a cut-off at 8 Å and a dielectric susceptibility of 3 was used for final minimization. Spectral analysis, peak picking and volume integration have been performed using the program AURELIA[32]; figures were generated with the program SYBYL (Tripos, Inc.).

Coordinates. The coordinates for the two structures have been deposited in the Protein Data Bank (accession codes 1b4g (for S-P 15,21) and 1b4i (for S-P 8)).

Acknowledgments
The authors would like to thank K.C. Holmes for continuous support, M. Geyer for technical help and J.P. Adelman, J. Maylie, J. Mosbacher and G. Yellen for helpful comments and reading of the manuscript. The work was supported by the Deutsche Forschungsgemeinschaft (Fa 332/2-1).

Correspondence should be addressed to B.F. *email: bernd.fakler@uni-tuebingen.de*

Received 9 July, 1998; accepted 29 October, 1998.

1. Greengard, P., Jen, J., Nairn, A.C. & Stevens, C.F. *Science* **253**, 1135–1138 (1991).
2. Huganir, R.L., Delcour, A.H., Greengard, P. & Hess, G.P. *Nature* **321**, 774–776 (1986).
3. Numann, R., Catteral, W.A. & Scheuer, T. *Science* **254**, 115–118 (1991).
4. Drain, P., Dubin, A.E. & Aldrich, R.W. *Neuron* **12**, 1097–1109 (1994).
5. Covarrubias, M., Wei, A., Salkoff, L. & Vyas, T.B. *Neuron* **13**, 1403–1412 (1994).
6. Beck, E.J., Sorensen, R.G., Slater, S.J. & Covarrubias, M. *J. Gen. Physiol.* **112**, 71–84 (1998).
7. Armstrong, C. & Bezanilla, F.J. *J. Gen. Physiol.* **70**, 567–590 (1977).
8. Hoshi, T., Zagotta, W.N. & Aldrich, R.W. *Science* **250**, 533–538 (1990).
9. Zagotta, W.N., Hoshi, T. & Aldrich, R.W. *Science* **250**, 568–571 (1990).
10. Murrell-Lagnado, R.D. & Aldrich, R.W. *J. Gen. Physiol.* **102**, 949–975 (1993).
11. Rettig, J. *et al. EMBO J.* **11**, 2473–2486 (1992).
12. Demo, S.D. & Yellen, G. *Neuron* **7**, 743–753 (1991).
13. Antz, C. *et al. Nature* **385**, 272–275 (1997).
14. Ruppersberg, J.P., Frank, R., Pongs, O. & Stocker, M. *Nature* **353**, 657–660 (1991).
15. Stephens, G.J. & Robertson, B. *J. Physiol.* **484**, 1–13 (1995).
16. Oliver, D., Hahn, H., Antz, C., Ruppersberg, J.P. & Fakler, B. *Biophys. J.* **74**, 2318–2326 (1998).
17. Johnson, L.N. & O'Reilly, M. *Curr. Opin. Struct. Biol.* **6**, 762–769 (1996).
18. Bundi, A. & Wüthrich, K. *Biopolymers* **18**, 185–297 (1979).
19. Lin, K., Rath, V.L., Dai, S.C., Fletterick, R.J. & Hwang, P.K. *Science* **273**, 1539–1541 (1996).
20. Russo, A., Jeffrey, P.D. & Pavletich, N.P. *Nature Struct. Biol.* **3**, 696–700 (1996).
21. Hoffman, D.A., Magee, J.C., Colbert, C.M. & Johnston, D. *Nature* **387**, 869–875 (1997).
22. Hille, B. *Ionic channels of excitable membranes* (Sinauer Associates Inc., Sunderland, Massachusetts; 1992).
23. Debanne, D., Guerineau, N.C., Gähwiler, B.H. & Thompson, S.M. *Nature* **389**, 286–289 (1997).
24. Fakler, B. *et al. Cell* **80**, 149–154 (1995).
25. Frank, R. & Gausepohl, H. *Modern methods in protein chemistry* (de Gruyter, Berlin, Federal Republic of Germany, 1988).
26. Freund, J. & Kalbitzer, H.R. *J. Biomol. NMR* **5**, 321–322 (1995).
27. Jeener, J. *J. Chem. Phys.* **71**, 4546–4553 (1979).
28. Aue, W.P., Bartholdi, E. & Ernst, R. *J. Chem. Phys.* **64**, 2229–2246 (1976).
29. Davis, D.G. & Bax, A. *J. Am. Chem. Soc.* **107**, 2820–2821 (1985).
30. Brünger, A.T. *X-PLOR (version 3.851) manual* (Yale University Press, New Haven, Connecticut, 1992).
31. Kirkpatrick, S., Gelatt, G.C. & Vecchi, M.P. *Science* **220**, 671–680 (1983).
32. Neidig, K.P. *et al. J. Biomol. NMR* **6**, 255–270 (1995).